Water as a Modifier in a Hybrid Coordination Network Glass

Sørensen, Søren Strandskov; Ren, Xiangting; Du, Tao; Traverson, Ayoub; Xi, Shibo; Jensen, Lars Rosgaard; Bauchy, Mathieu; Horike, Satoshi; Wang, John; Smedskjær, Morten Mattrup

Published in:
Small

DOI (link to publication from Publisher):
10.1002/smll.202205988

Publication date:
2023

Document Version
Publisher's PDF, also known as Version of record

NANO · MICRO small
www.small-journal.com

Water as a Modifier in a Hybrid Coordination Network Glass

*Søren S. Sørensen, Xiangting Ren, Tao Du, Ayoub Traverson, Shibo Xi, Lars R. Jensen, Mathieu Bauchy, Satoshi Horike, John Wang, and Morten M. Smedskjaer**

Chemical diversification of hybrid organic–inorganic glasses remains limited, especially compared to traditional oxide glasses, for which property tuning is possible through addition of weakly bonded modifier cations. In this work, it is shown that water can depolymerize polyhedra with labile metal–ligand bonds in a cobalt-based coordination network, yielding a series of nonstoichiometric glasses. Calorimetric, spectroscopic, and simulation studies demonstrate that the added water molecules promote the breakage of network bonds and coordination number changes, leading to lower melting and glass transition temperatures. These structural changes modify the physical and chemical properties of the melt-quenched glass, with strong parallels to the "modifier" concept in oxides. It is shown that this approach also applies to other transition metal-based coordination networks, and it will thus enable diversification of hybrid glass chemistry, including nonstoichiometric glass compositions, tuning of properties, and a significant rise in the number of glass-forming hybrid systems by allowing them to melt before thermal decomposition.

1. Introduction

Hybrid organic-inorganic networks, including 3D metal-organic frameworks (MOFs) and 1- or 2D coordination polymers (CPs), have opened new application areas within solid-state chemistry throughout the last few decades.[1,2] The materials typically consist of metal nodes connected by organic linkers, and in some cases include additional metallic-node centers, e.g., in perovskite structures.[3,4] The majority of the discovered structures are crystalline and typically synthesized by hydrothermal processes,[5] but recently it has been discovered that some members of this chemical family can form a stable liquid phase upon heating (prior to thermal decomposition), allowing subsequent supercooling into a glassy state.[6–9] This work has opened a new glass family,[10] notably distinct from the existing metallic, organic, and inorganic glasses, and with possible applications in, e.g., nuclear waste immobilization,[11] thermoelectrics,[4] gas separation,[12] and energy storage,[13] as well as the possibility to produce bulk-sized hybrid organic-inorganic samples (>1 cm^3) without grain boundaries.[14]

Although these hybrid glasses are chemically distinct from the traditional glass families, they share a number of structural similarities to chemically ordered network glasses (e.g., oxides), as the metallic nodes (for oxides typically Si, Ge, P; for hybrids typically transition metals) bridge through single oxygens and large organic linkers for oxide and hybrid glasses, respectively.[15] Similarly, the metal nodes in the two glass families share the same range of coordination numbers (typically 4–6).[15–17] However, there is a major difference in the discovery

S. S. Sørensen, X. Ren, T. Du, A. Traverson, M. M. Smedskjaer
Department of Chemistry and Bioscience
Aalborg University
Aalborg 9220, Denmark
E-mail: mos@bio.aau.dk

A. Traverson
Chemistry DER
University Paris-Saclay, ENS Paris-Saclay
Gif-Sur-Yvette 91190, France

S. Xi
Institute of Chemical & Engineering Sciences
Technology and Research (A*STAR)
Singapore 627833, Singapore

The ORCID identification number(s) for the author(s) of this article can be found under https://doi.org/10.1002/smll.202205988.

DOI: 10.1002/smll.202205988

L. R. Jensen
Department of Materials and Production
Aalborg University
Aalborg 9220, Denmark

M. Bauchy
Department of Civil and Environmental Engineering
University of California
Los Angeles, CA 90095, USA

S. Horike
Institute for Integrated Cell-Material Sciences
Institute for Advanced Study
Kyoto University
Kyoto 606-8501, Japan

J. Wang
Department of Materials Science and Engineering
National University of Singapore
Singapore 117574, Singapore

and design of new glasses. Hybrid glasses are typically made by melt-quenching or ball-milling a specific crystal or a mixture of crystals of which at least one should be meltable and thus "co-melt" the mixture.[18] Recent findings also suggest that eutectic points may be used to guide hybrid glass formation.[19] On the other hand, the compositions of oxide glasses are well known for allowing continuous composition adjustment through the addition of so-called modifiers or "fluxes" (e.g., alkali oxides), which result in the breakage of the continuous network structure of the pure network-forming oxide, thereby creating non-bridging oxygens, i.e., oxygens which will only covalently bond to one cationic node.[15] This leads to changes in the physical properties, for example lowering of the melting and glass transition temperatures, hence enabling melting at significantly lower temperatures.[15] The modifier addition in oxide glasses thus enables a significant chemical diversity that has led to a broad range of applications, from window glasses and touch-screen displays to nuclear waste immobilization, bioactive glasses, and pharmaceutical vials.[20] While some works have been devoted to co-melting and property tuning of MOFs and other coordination networks, e.g., through partial crystallization of glass and ionic liquid facilitated melting,[18,21,22] the lack of a universal method for modification of hybrid glasses is one of the main bottlenecks for exploiting the vivid potentials of this glass family.

In this work, we present experimental and computational evidence for water acting as a modifier in a transition metal-based bis-acetamide hybrid coordination network glass (HCNG) of composition $Co(hmba)_3[CoBr_4]$, where hmba: *N,N'*-1,6-hexamethylenebis(acetamide). While we focus on the $Co(hmba)_3[CoBr_4]$ system, we also confirm the effect of the modifier on other hybrid coordination networks when changing the bridging metal to Mn or the charge compensating anion to thiocyanate, i.e., for $Mn(hmba)_3[MnBr_4]$ and $Co(hmba)_3[Co(SCN)_4]$ systems, respectively. Here, we use the term "hybrid coordination network" instead of "metal-organic framework" to describe these systems as the latter may imply a 3D dimensionality as well as porosity, whereas the former designation better captures the bonding scheme in the studied systems.[17] Structurally, in the crystalline state, the $Co(hmba)_3[CoBr_4]$ system consists of octahedral Co^{2+} nodes connected through weak coordination bonds to uncharged hmba structures in a 2D layer-like structure, with noninterconnected charge compensating $[CoBr_4]^{2-}$ units situated in between network layers (see **Figure 1**a–c).[17,23] While this glass is water-soluble when being submerged in water, we show that careful water addition results in significant alteration of physical properties including the melting and glass transition temperatures. Both experiments and ab initio simulations show that water facilitates the breaking of the network-forming Co—O bonds

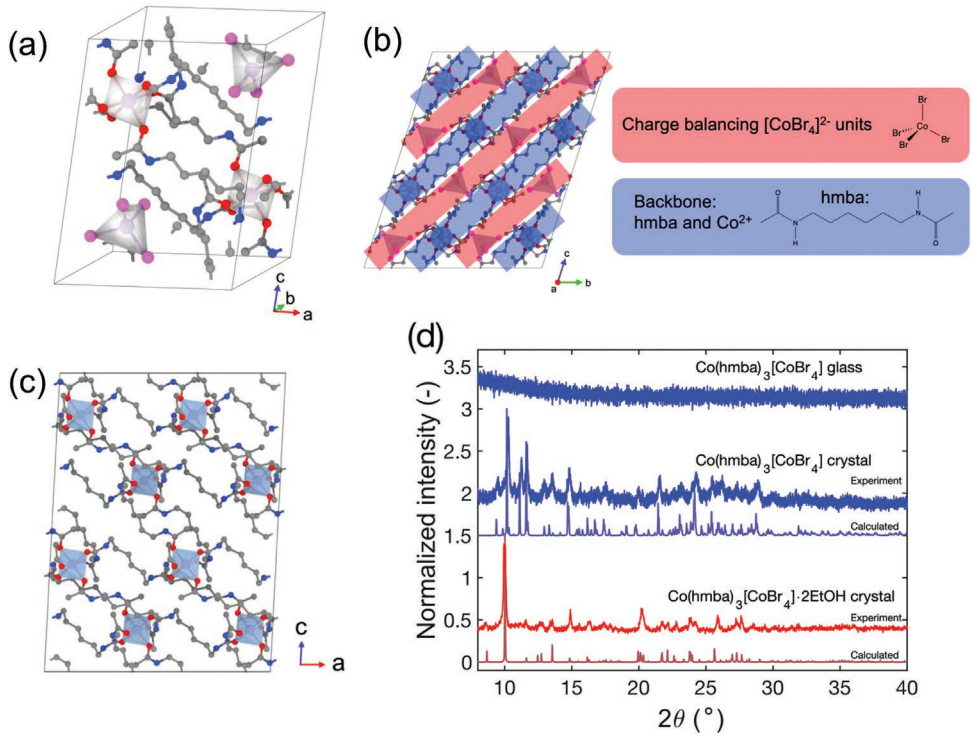

Figure 1. a) Unit cell of crystalline $Co(hmba)_3[CoBr_4]$ with highlights of Co tetrahedra and octahedra (shaded in gray), with the colored spheres representing carbon (grey), nitrogen (blue), oxygen (red), and bromine (pink) atoms. Hydrogens are omitted for clarity. b) Replicated $Co(hmba)_3[CoBr_4]$ structure overlaid with highlighting showing how Co^{2+} and hmba serve as the network part of the structure (blue), while $[CoBr_4]^{2-}$-tetrahedra are placed between the layers within the network (red). c) Depiction of a single layer of percolating hmba linkers and Co-octahedra. d) X-ray diffraction patterns of synthesized ethanol-containing crystals ($Co(hmba)_3[CoBr_4]\cdot 2EtOH$) and subsequently dried crystals ($Co(hmba)_3[CoBr_4]$) as well as the corresponding melt-quenched $Co(hmba)_3[CoBr_4]$ glass. The calculated reference spectra are based on the CIF files of ref. [23] which have also been deposited in the CCDC[24] with deposition numbers 120454 and 120455, respectively, where Mn is exchanged for Co. Arrows in (a–c) indicate crystallographic directions.

as well as alteration of the $[CoBr_4]^{2-}$ units, ultimately allowing for the tuning of glass properties within this glass family. We believe these findings pave a new avenue for tuning the melting temperatures of other hybrid crystals to allow them to melt before thermal decomposition, and hence allow the formation of a broader range of melt-quenched hybrid glass compositions.

2. Results and Discussion

2.1. Crystal Melting and Glass Formation: Effect of Water

The studied hybrid coordination network crystal ($Co(hmba)_3[CoBr_4]$) studied in the present work was synthesized following the procedure of ref. [17], creating single crystals with ethanol of composition $Co(hmba)_3[CoBr_4]\cdot 2EtOH$. The ethanol molecules were subsequently removed by prolonged storage under vacuum (<10 mbar) and moderate heating (≈30–40 °C), resulting in a polycrystalline powder that is isostructural to the $Mn(hmba)_3[MnBr_4]$ analog (as reported in ref. [23] and deposited in the Cambridge Crystallographic Data Centre (CCDC)[24] with deposition number 120454). The unit cell structure of $Co(hmba)_3[CoBr_4]$ (crystallizing in the *P*-1 space group with two unique Co sites, namely an octahedron and a tetrahedron) is presented in Figure 1a, while Figure 1b highlights the i) layer-like percolating network of Co and hmba-linkers and ii) interpenetrating $[CoBr_4]^{2-}$-tetrahedra positioned in the vacancies of the layered network. Figure 1c shows a single layer of the percolating hmba linkers and Co^{2+} octahedra. Finally, Figure 1d shows the measured X-ray diffraction (XRD) patterns of the crystal before and after drying together with simulated spectra of $Co(hmba)_3[CoBr_4]\cdot 2EtOH$ and $Co(hmba)_3[CoBr_4]$ structures as based on the unit cell structures of their Mn-analogs. Images of the two crystalline products are presented in Figure S1a (Supporting Information). The preparation of the $Co(hmba)_3[Co(SCN)_4]$ and $Mn(hmba)_3[MnBr_4]$ crystals follows a similar procedure (see Methods in Supporting Information) and XRD confirmation of their final structures is presented in Figure S2 (Supporting Information).[17] Furthermore, multiple signatures from the hmba ligands in the $Co(hmba)_3[CoBr_4]$ structure are confirmed by the X-ray photoelectron spectroscopy (XPS) data presented in Figure S3 (Supporting Information). For $Co(hmba)_3[CoBr_4]\cdot 2EtOH$, $Co(hmba)_3[CoBr_4]$, and $Mn(hmba)_3[MnBr_4]$ crystals, we observe an excellent reproduction of the XRD peaks, while some minor misalignment and possible amorphous and crystal impurities are observed for $Co(hmba)_3[Co(SCN)_4]$. However, we note that the expected reflections are observed (Figure 1d and Figure S2, Supporting Information) and that the calorimetric response (in terms of the values of T_m and T_g) nicely resembles the $Co(hmba)_3[Co(SCN)_4]$ system when compared to the results in a previous study (see Figure S4, Supporting Information).[17] For $Co(hmba)_3[CoBr_4]$, these results confirm the expected structural change upon storage and subsequent desolvation,[17,23] but we note that the signal-to-noise ratio likely indicates an increased degree of thermal fluctuations as well as partial amorphization upon desolvation of the $Co(hmba)_3[CoBr_4]\cdot 2EtOH$ structure.

The melting and subsequent glass formation has been described previously for both $Co(hmba)_3[CoBr_4]$ (see example picture of molten $Co(hmba)_3[CoBr_4]$ in Figure S1b, Supporting Information) as well as other bis-acetamide-containing HCNGs including $Co(hmba)_3[Co(SCN)_4]$ and $Mn(hmba)_3[MnBr_4]$.[17] Yet, here we demonstrate that the properties of these systems are highly sensitive to the water content. **Figure 2**a shows differential scanning calorimetry heating scans performed in sealed Al crucibles for the pristine $Co(hmba)_3[CoBr_4]$ crystal and glass with none or 7 wt% added water (i.e., ≈4.6 water molecules per bridging cobalt atom, which is significantly below the content needed to fully dissolve the sample in water), respectively. Upon water addition, the melting transition clearly becomes broader as it occurs over a larger range of temperature and ends at a significantly lower temperature (right part of Figure 2a).

Before initiating melting, we also tested the effect of water addition on the X-ray diffraction pattern of the $Co(hmba)_3[CoBr_4]$ crystal (Figure S5, Supporting Information). Upon the addition of 14 wt% water (the maximum concentration used in the present study), the intensities of the crystal reflections decrease, but no new crystalline species appear. This suggests that water may partially amorphize the crystal before the melting procedure, possibly explaining the apparent decrease in the melting enthalpy upon water addition. Apart from the melting temperature, the glass transition temperature also decreases significantly upon water addition (left part of Figure 2a). The dependence of the melting peak temperature (T_m) and glass transition temperatures (T_g) on water content in the $Co(hmba)_3[CoBr_4]$ system is shown in Figure 2b. Examples of the DSC scans used to extract the T_m and T_g values at different water contents are shown in Figures S6 and S7 (Supporting Information), respectively. The increase in water concentration significantly lowers the melting temperature from ≈110 °C to a constant value of ~70 °C at a water concentration of ~7 wt%, with no significant changes upon further water addition. As the samples were prepared in sealed Al crucibles, water could not escape from the system during heating. There is also no indication of free water in the crucibles based on the calorimetric data around 0 °C, suggesting that all the added water is incorporated into the hybrid coordination network. However, it is interesting to study the stability of the hydrated glasses upon re-heating in an open crucible. To this end, we prepared a glass with ~7 wt% water, giving a T_g value of around −20 °C. Upon reheating to 120 °C in an open Al crucible followed by a 10 min isothermal hold, the T_g values increases to ~7 °C (Figure S8, Supporting Information). In comparison, the T_g of the pristine (anhydrous) glass is ≈20 °C, i.e., partial but not full recovery toward the original T_g value occurs upon reheating.

Furthermore, to probe the universality of the effect of water on T_m and T_g within the hmba HCNG family, we also investigate the melting behavior of the $Co(hmba)_3[Co(SCN)_4]$ and $Mn(hmba)_3[MnBr_4]$ networks.[17] As presented in Figure S9 (Supporting Information), we find a very similar effect of decreasing T_m with increasing water content in these systems as that found for $Co(hmba)_3[CoBr_4]$, although the $Co(hmba)_3[Co(SCN)_4]$ crystal features a 3D rather than a 2D network.[17] In addition to the melting and glass transitions, we observed recrystallization in the $Mn(hmba)_3[MnBr_4]$ system upon heating slightly above T_g with subsequent remelting when the temperature was further increased. Notably, this recrystallization is significantly suppressed upon adding even small

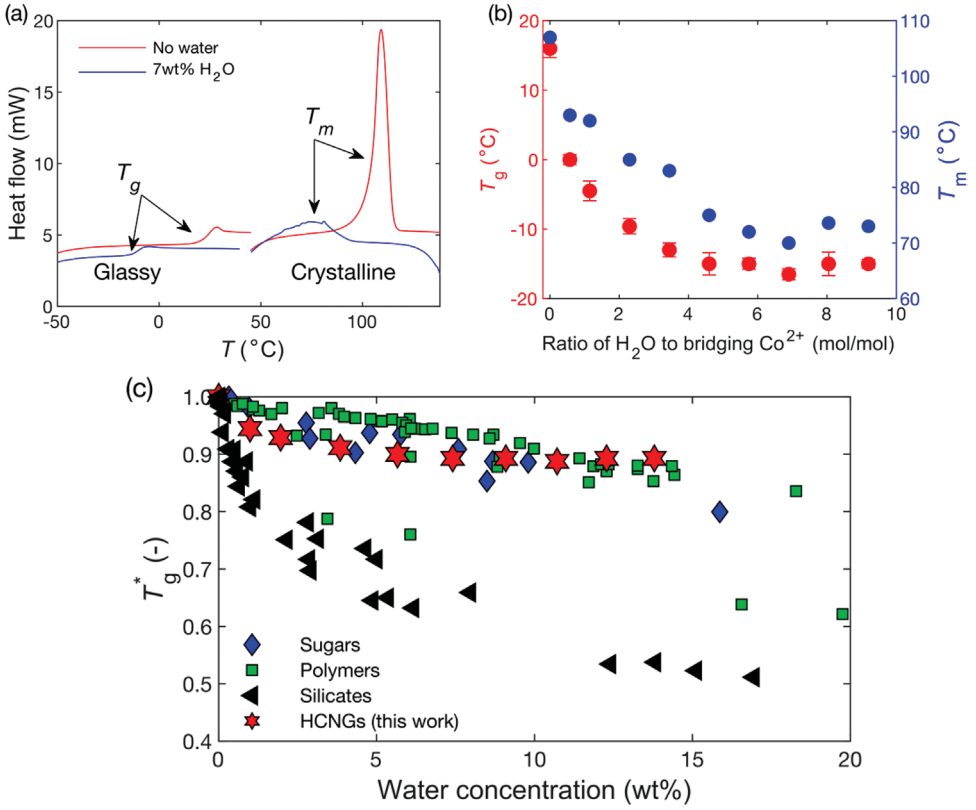

Figure 2. a) Differential scanning calorimetry heating scans of crystalline (right) and glassy (left) $Co(hmba)_3[CoBr_4]$. Results are shown for both a dry sample (red lines) and one with 7 wt% added water (blue lines), i.e., containing ≈4.6 water molecules per bridging cobalt atom. b) Melting and glass transition temperatures (T_m and T_g, reported as the peak and onset temperatures, respectively) of the $Co(hmba)_3[CoBr_4]$ as a function of the ratio of H_2O to bridging-Co (i.e., Co atoms bonded to hmba linkers). c) Reduced glass transition temperature ($T_g^* = T_g/T_g^{WF}$, scaled in Kelvin and where T_g^{WF} is the glass transition temperature of the water-free glass) of the $Co(hmba)_3[CoBr_4]$·water glasses at different water concentrations as well as of several different sugars, organic polymers, and silicate glasses as obtained from refs. [25–27].

amounts of water (see Figure S10, Supporting Information). As such, water addition may be used to increase the glass forming ability, which in some HCNGs has been observed to be low,[22] or tune the properties of mixed glass-crystal phases. In summary, these observations clearly confirm the universality of the water effect on the melting within the present hmba-based glass family. However, in the remaining part of this article, we focus on the $Co(hmba)_3[CoBr_4]$ system as it features the best glass-forming ability and thus serves as a good model system for understanding the mechanism of the water interaction with the hybrid network.

Considering the $Co(hmba)_3[CoBr_4]$ system, we find a decrease in its glass transition temperature from a pristine value of 16 °C to -17 °C for the highest water content studied, which corresponds to nine water molecules per bridging Co atom, where bridging-Co refers to Co atoms bonded to hmba linkers. Notably, a significant initial decrease followed by stabilization is observed for both T_m and T_g. Specifically, T_m and T_g reach a constant value when around three to four water molecules per bridging-Co have been added. Interestingly, this is equivalent to the ratio of bridging-Co to hmba in the system. Thus, at the water concentration of T_g-convergence, one water molecule per hmba linker is present. Based on this analysis and considering the chemical environment of the percolating network, i.e., Co-nodes connected by bidentate hmba-linkers through Co—O coordination bonds, the monodentate water species thus appear to replace the bridging carbonyl oxygens around the Co centers. This leads to a fully depolymerized network of Co atoms surrounded by a distribution of hmba-linkers and water molecules, while the $[CoBr_4]^{2-}$-tetrahedra would remain largely intact. As such, this behavior is equivalent to water-based modifier addition in the HCNG system, which, to our knowledge, has not previously been reported for hybrid glasses.

To test the state of the trapped water in the structures, we have investigated the water evaporation from the dry and hydrated glasses (i.e., containing 0, 7, and 14 wt% water, equivalent to 0, 4.6, and 9.2 H_2O per bridging Co, respectively). These experiments were done in open crucibles by thermogravimetric analysis (Figure S11, Supporting Information), while we note that the initial water incorporation was done in sealed crucibles. We find that nearly all the added water is released upon heating and that evaporation is initiated already at ~50 °C (upon contact with a dry He atmosphere). The sample with 14 wt% water exhibits a faster water release at lower temperatures compared with the 7 wt% water sample. This suggests weaker bonding of water at higher water concentrations. That is, some water may not be interacting with the coordinating Co-octahedra and thus either weakly bond in the depolymerized hybrid

coordination structure or react with the $[CoBr_4]^{2-}$ units. These observations agree with the stabilization of the T_g and T_m values at high water contents (Figure 2b).

The water-induced depolymerization and decrease in T_g have been observed in other glassy systems, including silicates, organic polymers, and sugars. To compare the extent of the decrease, we plot the reduced glass transition temperature ($T_g^* = T_g(T_g^{WF})^{-1}$, where T_g^{WF} is the glass transition temperature of the water-free glass) as a function of water content in Figure 2c. Results are shown for the present $Co(hmba)_3[CoBr_4]$ glass well as various systems available from literature.[25–27] Water addition has a pronounced effect on the T_g of the inorganic silicates and polymers, with a decrease in their T_g by ~50% when adding 10–14 wt% water. This contrasts the behavior of the majority of the sugars and polymers as well as the present $Co(hmba)_3[CoBr_4]$ HCNG, which exhibit only a minor (~10–15%) reduction in T_g in the same water concentration range. Interestingly, the water-containing $Co(hmba)_3[CoBr_4]$ HCNGs also appear to feature a more converged T_g (i.e., T_g is constant upon increasing water content) compared to other organic and inorganic systems upon water addition. This is likely because water significantly outnumbers the number of bridging Co atoms at a relatively low water concentration (~5–10 wt%), creating a glassy system controlled by weaker cohesive forces and hydrogen bonds. In contrast, the anhydrous system consists of the highly crosslinked (yet rather weak) Co-hmba network.

To further clarify the glass transition behavior of the $Co(hmba)_3[CoBr_4]$ glasses, we performed annealing experiments at $0.9T_g$ of both pristine and hydrated samples. Based on the DSC measurements of these samples, we find for both the pristine and hydrated glasses that their fictive temperatures (T_f, determined in a similar manner as T_g from calorimetry, yet with varying heating rates) decrease, and the endothermic overshoot of the glass transition increases with annealing duration (Figure S12, Supporting Information). This is consistent with previous findings for other glass families[28,29] and is a consequence of the decrease in the overall enthalpy of the system through the hopping between metastable states and, upon such heating, into local minima of the potential energy surface.[30] Additionally, we determined the liquid fragility (m), which quantifies the extent of non-Arrhenius temperature dependence of viscosity at T_g (see Supporting Text for an introduction to the concept of liquid fragility as well as the method to determine it). This was done on both pristine and hydrated glasses using a DSC-based method.[31] Specifically, glasses were heated from below to above T_g at a range of heating rates (5, 10, 15, 20, 25, and 30 K min^{-1}) and the shift in fictive temperature was recorded (see Figure S13, Supporting Information for calorimetric scans of anhydrous and hydrates glasses at various heating rates). This gave m values of 42 ± 4 and 47 ± 6 for the pristine and hydrated glass, respectively. This is in the same range as many modified oxide and metallic glass-forming systems ($m \approx 30$–70),[32,33] but considerably lower than most organic systems[31] and higher than the hybrid ZIF-62 ($m = 23$)[34] as well as pure SiO_2 ($m = 20$)[35] glasses. We note that assigning a structural origin to these differences in fragility is challenging, given that fragility is determined by the temperature derivative of atomic degrees of freedom.[36]

2.2. Spectroscopic Analyses

To understand these changes in melting and glass transition behavior upon water addition, we conducted a series of spectroscopic analyses on the water-containing $Co(hmba)_3[CoBr_4]$ HCNGs, including in situ Raman spectroscopy measurements during the crystal melting and a subsequent cooling/heating cycle (Figure S14, Supporting Information), and ex situ FT-IR spectroscopy measurements (Figure S15, Supporting Information). In agreement with the in situ FT-IR data reported in ref. [17], we find no apparent changes in our ex situ FT-IR measurements upon the glass formation in the anhydrous system except for some peak broadening. In the hydrated glass, we find a stronger intensity and a broad band in the frequency range of 3000–3700 cm^{-1}, indicating the presence of water in the hydrated glass. In the in situ Raman spectroscopy measurements, we find that a peak at ~1611 cm^{-1} ascribed to the carbonyl vibration in hmba (based on previous studies of Co–acetamide complexes[37]) is significantly reduced around the melting temperature (Figure S14a, Supporting Information), but then overlaps with nearby peaks without resharpening in the glassy state (Figure S14d, Supporting Information). This suggests that the carbonyl group is directly involved in the melting transition and in agreement with the expected variation in the chemical environment of the carbonyl unit relative to Co (breaking of bonds and variation in bond angles and lengths) in the molten and glass states compared to the crystal. In turn, this would affect the distribution of the specific vibration frequency of the carbonyl bonds. Such broadening of otherwise sharp crystalline Raman bands upon melting is well known in other systems, e.g., silicates.[38]

To further probe any structural changes around the Co atoms, we measured the visible absorption spectra of the pristine and hydrated glasses (**Figure 3**a). We were unable to quantify the used film thickness and hence the absorption coefficient due to differences in thickness across the film. However, we find that higher water content leads to smaller absorption. The large band around 6–700 nm present in all samples can be assigned to the crystal field splitting in $[CoBr_4]^{2-}$, where Br^- ligands are tetrahedrally coordinated to Co-centers, as[39] i) Br^- is in the lowest splitting part of the spectrochemical series, and ii) lower coordination is known to induce lower splitting. This interpretation agrees well with previous absorption spectra of tetrahedral $[CoBr_4]^{2-}$ in a tetrabutylammonium $[CoBr_4]^{2-}$ complex.[40] As such, the octahedral Co atoms surrounded by carbonyls should absorb at smaller wavelengths (higher energies) due to their expected larger splitting (based on the spectrochemical series) and higher coordination state, yet most likely with a significantly lower absorption coefficient (possibly by several orders of magnitude[41]) and therefore it cannot be observed. As such, the minor changes in the normalized absorption spectrum suggest that the $[CoBr_4]^{2-}$ units remain relatively stable both in the pristine and hydrated glasses, but based on the observed decrease in absorption, their abundancy likely decreases.

2.3. Molecular Dynamics Simulations

The melting mechanism of the $Co(hmba)_3[CoBr_4]$ system as well as that with 0, 1, 2, or 3 water molecules added was

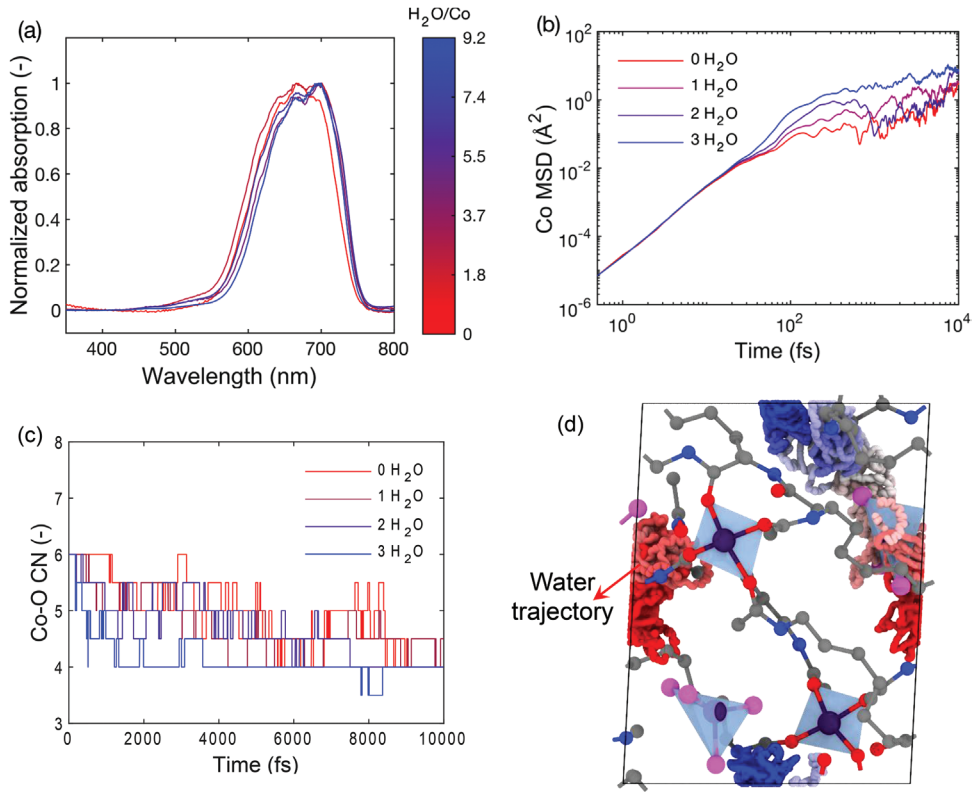

Figure 3. a) Normalized visible absorption spectra of $Co(hmba)_3[CoBr_4]$ HCNGs with varying water content (see colorbar). b) Simulated mean square displacement (MSD) of Co atoms in the $Co(hmba)_3[CoBr_4]$ system at 1000 K with 0, 1, 2, or 3 water molecules in the unit cell structure. Note the logarithmic axes. c) Simulated average coordination number (CN) of the Co—O correlation in structures containing 0, 1, 2, or 3 water molecules. d) Trace of one water molecule's trajectory over 10 ps of simulation time at 1000 K, where blue refers to the initial position and red to the final position. The remaining part of the structure is shown as the final frame. Note the movement across the periodic boundaries.

further studied by ab initio molecular dynamics simulations. The procedure generally follows that of a previous work studying the melting of a Mn^{2+}-based hybrid perovskite system.[4] While our simulations provide new insights as shown below, we note that the short simulation timescales and lack of quenching to the glass state (due to the very high computational cost) reduce our possibilities of observing chemical species and making direct comparisons to the experimental findings. First, we consider the dynamics of the pristine, water-free crystal structure (as obtained from its CIF file) at temperatures of 500, 1000, and 1500 K to calculate the mean square displacement (MSD). The results are shown in Figure 3b for Co MSD at 1000 K for different water contents and in Figure S16 (Supporting Information) for both Co and Br MSD at the different temperatures. The simulations at 500 K present solid-like behavior (i.e., constant value of MSD), while the simulations at 1500 K present a liquid/gas-like behavior (i.e., increasing MSD with time). The simulations at 1000 K exhibit behavior in-between these extrema, thus representing an initiation of melting. We further confirmed this through calculation of the Lindemann ratio (Δ), i.e., the ratio of the estimated amplitude of the atomic vibrations divided by the bond length[42,43] of the Co—O bonds. As shown in the inset of Figure S16a (Supporting Information), Δ increases from ~0.10 to ~0.18 when the temperature is increased from 500 to 1500 K. Generally, melting is considered to occur when Δ reaches a value of around 0.10–0.15,[42,43] matching the values from the simulation data at 1000 K. By adding water to the $Co(hmba)_3[CoBr_4]$ system at 1000 K, the Co MSD increases more rapidly with time (Figure 3b), suggesting that water promotes the melting process. The same trend that the MSD increases with both temperature and water content is also found for Br (Figure S16b,c, Supporting Information).

The melting process of the $Co(hmba)_3[CoBr_4]$ system is also investigated through analysis of the simulated coordination numbers (CNs) of the two different Co-centers (i.e., the Co—O and Co—Br CNs). Interestingly, we find that the CN of the Co—O and Co—Br correlations differ significantly (see Figure 3c for Co—O and Figure S17, Supporting Information for Co—Br). We note that the stepwise nature of the data in these figures is due to the small number of Co atoms in each simulated box. Upon initializing dynamics at 1000 K of the crystalline system with 0, 1, 2, or 3 water molecules, we observe a major decrease in the Co—O CN (i.e., the network percolating species) from 6 to ~4 within the first 10 ps. This decrease in CN is found to be promoted by the presence of water, as seen from the more rapid decrease of CN in the first picosecond of the simulation with the largest amount of water. To showcase this, we have fitted the data to a stretched exponential decay function,

$$\mathrm{CN}(t) = a e^{-\left(\frac{t}{t_0}\right)^b} + (6 - a) \quad (1)$$

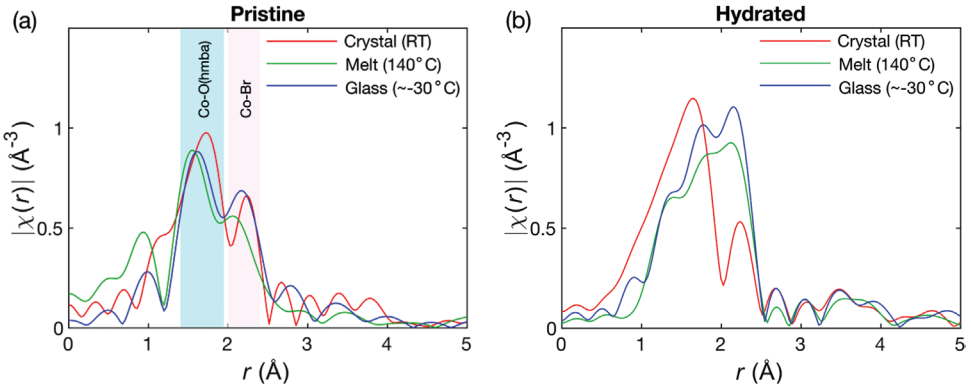

Figure 4. In situ Fourier transformed extended X-ray absorption fine structure (FT-EXAFS) spectra of a) pristine and b) hydrated (~14 wt% H_2O) $Co(hmba)_3[CoBr_4]$ systems in the crystalline state (red), molten phase at 140 °C (green), and glassy state at approximately −30 °C (blue). Areas for the approximate radial distances corresponding to cobalt coordinating to oxygens from hmba as well as Br are shaded in blue and pink, respectively.

where a is the decay of CN, b is an exponential fitting parameter related to the rapidness of the decay, and t_0 is the time needed to reach 63.2% of the expected decay, a. We restrict $0 \leq a \leq 2$ and note how Equation (1) ensures that the fit is initiated at CN(0) = 6. We show the obtained fits in Figure S18a–d (Supporting Information) and the derived parameters in Table S1 (Supporting Information). Generally, the time constant is found to decrease with increasing water content (Figure S18e, Supporting Information), highlighting how water acts to enhance the decoordination of hmba linkers towards the molten state.

In contrast to the Co−O centers, the Co−Br tetrahedra exhibit only minor deviations from the initial four-fold coordinated state caused by the high temperature. This persistence of the tetrahedral state is found to be largely independent of the water content (Figure S17, Supporting Information), but we note that the change in CN is more pronounced at higher water content. Figure 3d illustrates the movement of a water molecule inside the structure at 1000 K, highlighting how water explores multiple parts of the structural space, including both the Co−O octahedra as well as the Co−Br tetrahedra. However, the water molecule does not seem to directly bond to neither Co centers nor replace the oxygens in hmba or the bromide ions in the molten state. This is supported by calculations of the time-resolved bond distance between the oxygens from water and the Co atoms in the structure, with separation distances surpassing 3 Å (Figure S19, Supporting Information) in contrast to the network-forming Co−O and interconnected Co−Br bonds, exhibiting bond distances in the range of 1.9–2.5 Å (Figures S20–S23, Supporting Information).

2.4. Co Environment Probed by EXAFS

To complement the ab initio simulations and provide real space temperature-resolved structural information of the $Co(hmba)_3[CoBr_4]$ hybrid coordination network system in both the crystalline, molten, and glassy states, we have performed in situ extended X-ray absorption fine structure (EXAFS) measurements (see raw data in Figure S24, Supporting Information) collected at the Co K-edge to assess the local environment of Co atoms in samples. The Fourier-transformed extended X-ray absorption fine structure (FT-EXAFS) spectra are shown in **Figure 4** for both the pristine (Figure 4a) and hydrated (Figure 4b, 14 wt% water) systems in the crystalline (red), molten (green), and glassy states (blue). We note that the presented FT-EXAFS spectral peaks are shifted by around −0.5 Å due to an uncorrected phase shift, which is a common feature in EXAFS data. In the water-free system, the cobalt environment features a bimodal distribution of bond lengths, with the shortest one corresponding to Co−O (below 2 Å) and the longer one to the Co−Br distance (above 2 Å). Upon heating to 140 °C, we find a decrease in the overall peak area of both the Co−O and Co−Br correlations, suggesting a decrease in the CNs and an increase in thermal disorder for both Co environments in the structure. We note that the simulations mainly showed breakage of the Co−O bonds, but this may reflect the general limits in terms of simulation time. Furthermore, we find that the Co−Br bonds appear to be re-established when cooling into the glassy state, while the Co−O bonds appear to be permanently shortened and with a smaller CN (see Figure 4a, blue curve). This is consistent with the persistent blue color from the $[CoBr_4]^{2-}$ centers observed in the optical absorption spectra (Figure 3a).

Significant changes in the FT-EXAFS spectra are observed upon water addition to the $Co(hmba)_3[CoBr_4]$ system (Figure 4b). First, considering the crystalline state with added water, the relative intensity of the Co−O to the Co−Br peak is significantly increased when adding water (see direct comparison in Figure S25a, Supporting Information) and a new shoulder peak around 1.4 Å seems to appear. This may be because water already affects the Co−O octahedra even before the system enters the molten phase, as also suggested by the partial amorphization found upon hydration of the crystal (Figure S5, Supporting Information). Yet, the decrease in the relative intensity of the Co−Br peak would suggest that this species is partially removed even in the non-heated state. This suggests that some of the Co−Br tetrahedra are hydrated, possibly forming a new Co species (likely fully or partially surrounded by H_2O and Br) that gives rise to the new shoulder peak. Such species have previously been suggested to exist.[44]

Now, upon heating to 140 °C (green curve in Figure 4b), the local geometry of Co is further altered, with more significant

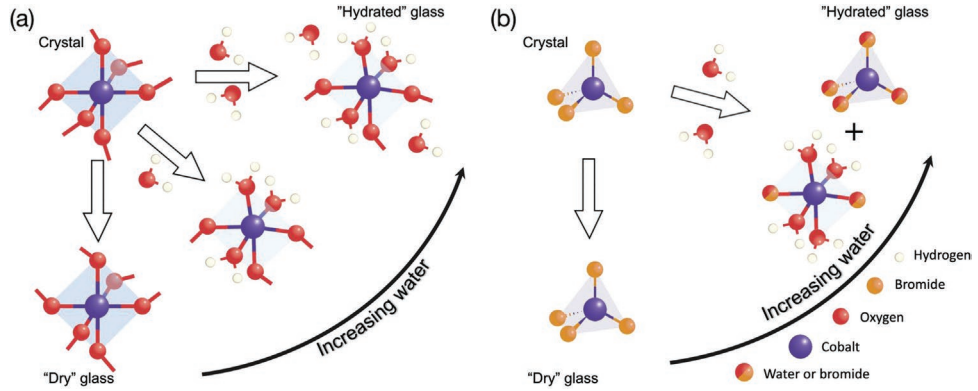

Figure 5. Proposed structure of the a) octahedral Co—O and b) tetrahedral $[CoBr_4]^{2-}$ sites in the water-free crystal (top left) and the glasses after melt-quenching with different amounts of added water. Bottom left: no water; top right: excess water beyond what causes full depolymerization of the network. Cobalt, oxygen, bromine, and hydrogen are represented as violet, red, yellow, and white spheres, respectively. Note the suggested possibility of mixed water/bromide octa- and tetrahedra in (b).

changes in the coordination environments as compared to the anhydrous case (Figure 4a). An apparent trimodal distribution is observed. We are not able to unambiguously assign the different signals to specific chemical species. However, we note the appearance of a new peak around 1.4 Å, which was previously visible as a shoulder in the hydrated crystalline system. Simultaneously the peak at ≈1.8 Å appears to be shifted to larger distances compared to the anhydrous system (Figure 4a). The observed splitting might be due to a variation in the coordination number of Co as well as a modified ligand distribution incorporating water. This is supported by previous studies, suggesting that $[Co(H_2O)_4]^{2+}$ species can be present under some conditions, e.g., at elevated temperatures,[45] and featuring a shortened bond length of 2.0–2.1 Å[46] (i.e., slightly shorter than the bond-length expected in Co—O(hmba) of 2.1–2.2 Å[17,47]). Similarly, as also suggested in the case of the hydrated crystal, mixed halide/water species likely exist in the obtained melt and glass.[44] This interpretation is based on how the crystalline Co—Br peak (shown above 2 Å) increases in intensity upon melting and glass formation in the hydrated sample (Figure 4b). This would suggest that the coordination number increases, possibly by the inclusion of water to form mixed octahedra with Br^- and H_2O ligands.

Such mixed coordination environments for Co—Br—H_2O have previously been observed for weak aqueous solutions of $CoBr_2$ at elevated temperatures.[44] Based on the measured UV–vis absorption spectra (Figure 3a), some $[CoBr_4]^{2-}$ centers likely remain intact, but feature a decrease in the fraction of this species. The latter is consistent with the general observation of lower UV–vis absorption with higher water content. That is, the percolating Co-hmba octahedra as well as the $[CoBr_4]^{2-}$ species feature a minor decrease in coordination upon melting in the anhydrous state. Yet upon cooling into the glass state, the $[CoBr_4]^{2-}$ species reform while the Co—O(hmba) network remains in a liquid-like state. In contrast, adding water to the crystal seems to slightly remove $[CoBr_4]^{2-}$ species, likely forming fully or partially hydrated tetrahedra. Upon heating, the Co—O(hmba) bonds are also altered by full or partial exchange with water molecules, while the $[CoBr_4]^{2-}$ units appear to be partially exchanging Br^- anions for water ligands while also partially adopting an octahedral state.

2.5. Melting Mechanism

Finally, based on the performed simulations and experiments, we propose a melting mechanism of the $Co(hmba)_3[CoBr_4]$ system with and without water addition, which is expected to also apply to other transition metal-based bis-acetamide hybrid coordination networks. First, upon heating of the anhydrous system, the labile bonds between Co and O in hmba (i.e., the red spheres in **Figure 5**a) tend to break, leading to a decrease in the overall network connectivity and ultimately the formation of a molten state. This is accompanied by minor breakage of the tetrahedral $[CoBr_4]^{2-}$ units. Upon cooling this liquid into the solid glass state, the $[CoBr_4]^{2-}$ units reform, while the Co—O network undergoes partial reformation (Figure 5a,b). By the addition of water to the crystal, the temperature-induced decoordination process is dramatically enhanced.

In the hydrated system, the Co—O(hmba) bonds likely break much more and some hmba are ultimately replaced by water molecules in the glassy state (Figure 5a). Furthermore, the addition of water causes the $[CoBr_4]^{2-}$ centers to adopt new geometries to allow for the full or partial addition of water into tetrahedral or octahedral states (Figure 5b). Ultimately, we suggest that when water replaces the oxygens of hmba, dangling organic motifs (i.e., hmba only coordinating to one Co center) are created as shown by the significant reduction in the T_g from 16 °C to -15 °C for the fully polymerized and fully depolymerized glass structures, respectively. Last, when adding more water than what causes full depolymerization, it is found that water bonds less tightly, suggesting that water has another bonding mechanism, likely related to the hydration of the $[CoBr_4]^{2-}$ centers. We note that only octahedral configurations are presented in Figure 5a, but that these are most likely accompanied by four- (and possibly five-) fold coordinated Co centers. In crystallography, such nonuniform distribution in hydration and coordination numbers are generally considered to be defects in the perfect crystal and hence not easily described (although commonly handled through, e.g., partial occupancies). However, such distributions of, e.g., coordination environments are intrinsic to the molten and glassy states.[15]

The fundamental melting (and glass formation) mechanism is similar to that of other known hybrid systems, namely ZIFs[16,42] and hybrid perovskites,[4] involving the breakage (and full or partial reformation) of the coordination network upon melting and subsequent quenching into the glassy state. As such, water addition limits the reformation of the initial network-connecting species, in agreement with the lack of recrystallization upon hydration in the $Mn(hmba)_3[MnBr_4]$ glass as shown in Figure S10 (Supporting Information). In oxide glass science, such elements are termed as "modifiers." The effect observed in this work, as studied in detail for $Co(hmba)_3[CoBr_4]$ but also confirmed for $Co(hmba)_3[Co(SCN)_4]$ and $Mn(hmba)_3[MnBr_4]$ systems, is therefore mechanistically different from the recent work of vitrification by desolvation.[48,49] We believe that the proposed structural mechanism is not unique to the systems studied in this work and may also find usefulness for, e.g., the much-studied ZIFs where much work has been devoted to lowering the melting temperature and viscosity[50] or other systems prone to react with water. As such, the ability to incorporate modifiers would be of great usefulness to push the field forward.

As reflected from the observed water-induced decrease in T_m and T_g (Figure 2b and Figures S6, S7, and S9, Supporting Information), the resulting glass properties are expected to exhibit similar large changes upon inclusion of water. From traditional rigidity considerations, the depolymerization of a network greatly reduces, e.g., its hardness and elastic moduli.[51–53] Such change may be useful depending on the application, but as hybrid glasses are generally soft and flexible,[14,54] further reducing the mechanical moduli may be disadvantageous. Similarly, chemical durability may be heavily impacted by modifier addition as in the case of oxide glasses, where modifiers can both enhance or reduce corrosion resistance depending on the chemistry of the glass and the corrosion conditions.[55] Similarly, it is also possible that modifiers in hybrid glasses could increase, e.g., T_g, by introducing stronger bonds or higher-coordinated species in the modified glass network. Such effect is well known in the case of for example borate glasses,[56] but has not yet been observed in hybrid glasses. Water (or other "modifier") addition may thus serve as a method for tweaking the properties of hybrid glasses, similar to the case of oxide glasses. Moreover, the described depolymerization could allow more hybrid and MOF crystals to melt before they thermally decompose, thus dramatically expanding the range of hybrid glass formation.

3. Conclusion

We have shown that water addition to a cobalt-based hybrid coordination network crystal leads to a significant decrease in its melting point and glass transition temperature significantly. Through calorimetric, spectroscopic, diffraction, XAFS, and simulation methods, we have proposed a mechanism for the water-promoted breakdown of the internal network of Co^{2+} ions and bis-acetamide organic linkers, with a partial redistribution of the $[CoBr_4]^{2-}$ centers. The former is obtained by replacing labile Co—O bonds from the organic ligand with coordination to water molecules. We also probed the effect of water addition on the melting behavior of two related hybrid coordination network systems with exchanged transition metals and charge balancing anions, showing a similar decrease in melting temperature and thus confirming the universality of the mechanism for other hmba-based hybrid coordination network glass systems. This mechanism resembles that of water and other network "modifiers" in traditional oxide glass-forming systems, where such structural modification is used to design and tune glass properties for industrial applications. As such, the present results pave the way for a significant expansion of the meltable and glass-forming hybrid systems as well as substantial non-stoichiometric chemical diversification of these systems.

Supporting Information

Supporting Information is available from the Wiley Online Library or from the author.

Acknowledgements

S.S.S., X.R., and T.D. contributed equally to this work. This work was supported by the Independent Research Fund Denmark (0136-00011), the China Scholarship Council (201906250152), and the European Union's Horizon 2020 research and innovation programme (Marie Skłodowska-Curie grant agreement No. 101018156). The authors also acknowledge EuroHPC for computing resources on the Vega HPC (EU2010PA6249) as well as the XAFCA beamline of Singapore Synchrotron Light Source (SSLS) for providing the facilities necessary for conducting the experimental X-ray absorption spectroscopy measurements. The SSLS is a National Research Infrastructure under the National Research Foundation, Singapore. M.B. acknowledges funding from the National Science Foundation (grants DMR-1928538 and DMR-1944510).

Conflict of Interest

The authors declare no conflict of interest.

Data Availability Statement

The data that support the findings of this study are available from the corresponding author upon reasonable request.

Keywords

coordination networks, glass modifiers, hybrid glasses, melting, water

Received: September 29, 2022
Revised: December 21, 2022
Published online: January 26, 2023

[1] R. J. Kuppler, D. J. Timmons, Q. R. Fang, J. R. Li, T. A. Makal, M. D. Young, D. Yuan, D. Zhao, W. Zhuang, H. C. Zhou, *Coord. Chem. Rev.* **2009**, *253*, 3042.
[2] H. Furukawa, K. E. Cordova, M. O'Keeffe, O. M. Yaghi, *Science* **2013**, *341*, 1230444.
[3] A. Singh, M. K. Jana, D. B. Mitzi, *Adv. Mater.* **2021**, *33*, 2005868.

[4] B. K. Shaw, A. R. Hughes, M. Ducamp, S. Moss, A. Debnath, A. F. Sapnik, M. F. Thorne, L. N. McHugh, A. Pugliese, D. S. Keeble, P. Chater, J. M. Bermudez-Garcia, X. Moya, S. K. Saha, D. A. Keen, F. X. Coudert, F. Blanc, T. D. Bennett, *Nat. Chem.* **2021**, *13*, 778.
[5] K. S. Park, Z. Ni, A. P. Cote, J. Y. Choi, R. Huang, F. J. Uribe-Romo, H. K. Chae, M. O'Keeffe, O. M. Yaghi, *Proc. Natl. Acad. Sci. USA* **2006**, *103*, 10186.
[6] T. D. Bennett, J. C. Tan, Y. Yue, E. Baxter, C. Ducati, N. J. Terrill, H. H. M. Yeung, Z. Zhou, W. Chen, S. Henke, A. K. Cheetham, G. N. Greaves, *Nat. Commun.* **2015**, *6*, 8079.
[7] T. D. Bennett, Y. Yue, P. Li, A. Qiao, H. Tao, N. G. Greaves, T. Richards, G. I. Lampronti, S. A. T. Redfern, F. Blanc, O. K. Farha, J. T. Hupp, A. K. Cheetham, D. A. Keen, *J. Am. Chem. Soc.* **2016**, *138*, 3484.
[8] D. Umeyama, N. P. Funnell, M. J. Cliffe, J. A. Hill, A. L. Goodwin, Y. Hijikata, T. Itakura, T. Okubo, S. Horike, S. Kitagawa, *Chem. Commun.* **2015**, *51*, 12728.
[9] L. Frentzel-Beyme, M. Kloß, P. Kolodzeiski, R. Pallach, S. Henke, *J. Am. Chem. Soc.* **2019**, *141*, 12362.
[10] N. Ma, S. Horike, *Chem. Rev.* **2022**, *122*, 4163.
[11] T. D. Bennett, P. J. Saines, D. A. Keen, J. C. Tan, A. K. Cheetham, *Chem. - Eur. J.* **2013**, *19*, 7049.
[12] Y. Wang, H. Jin, Q. Ma, K. Mo, H. Mao, A. Feldhoff, X. Cao, Y. Li, F. Pan, Z. Jiang, *Angew. Chem., Int. Ed.* **2020**, *59*, 4365.
[13] G. Jiang, C. Qu, F. Xu, E. Zhang, Q. Lu, X. Cai, S. Hausdorf, H. Wang, S. Kaskel, *Adv. Funct. Mater.* **2021**, *31*, 2104300.
[14] T. To, S. S. Sørensen, M. Stepniewska, A. Qiao, L. R. Jensen, M. Bauchy, Y. Yue, M. M. Smedskjaer, *Nat. Commun.* **2020**, *11*, 2593.
[15] A. K. Varshneya, *Fundamentals of Inorganic Glasses*, Elsevier, Amsterdam **2013**.
[16] R. S. K. Madsen, A. Qiao, J. Sen, I. Hung, K. Chen, Z. Gan, S. Sen, Y. Yue, *Science* **2020**, *367*, 1473.
[17] M. Liu, R. D. McGillicuddy, H. Vuong, S. Tao, A. H. Slavney, M. I. Gonzalez, S. J. L. Billinge, J. A. Mason, *J. Am. Chem. Soc.* **2021**, *143*, 2801.
[18] L. Longley, S. M. Collins, S. Li, G. J. Smales, I. Erucar, A. Qiao, J. Hou, C. M. Doherty, A. W. Thornton, A. J. Hill, X. Yu, N. J. Terrill, A. J. Smith, S. M. Cohen, P. A. Midgley, D. A. Keen, S. G. Telfer, T. D. Bennett, *Chem. Sci.* **2019**, *10*, 3592.
[19] N. Ma, N. Horike, L. Lombardo, S. Kosasang, K. Kageyama, C. Thanaphatkosol, K. Kongpatpanich, K. I. Otake, S. Horike, *J. Am. Chem. Soc.* **2022**, *144*, 18619.
[20] J. E. Shelby, *Introduction to Glass Science and Technology*, The Royal Society Of Chemistry, London **2005**.
[21] V. Nozari, C. Calahoo, J. M. Tuffnell, D. A. Keen, T. D. Bennett, L. Wondraczek, *Nat. Commun.* **2021**, *12*, 5703.
[22] M. Liu, A. H. Slavney, S. Tao, R. D. Mcgillicuddy, C. C. Lee, M. B. Wenny, S. J. L. Billinge, J. A. Mason, *J. Am. Chem. Soc.* **2022**, *144*, 22262.
[23] D. M. L. Goodgame, D. A. Grachvogel, I. Hussain, A. J. P. White, D. J. Williams, *Inorg. Chem.* **1999**, *38*, 2057.
[24] C. R. Groom, I. J. Bruno, M. P. Lightfoot, S. C. Ward, *Acta Crystallogr* **2016**, *72*, 171.
[25] B. C. Hancock, G. Zografi, *Pharm. Res.* **1994**, *11*, 471.
[26] H. Z. Cummins, H. Zhang, J. Oh, J. A. Seo, H. K. Kim, Y. H. Hwang, Y. S. Yang, Y. S. Yu, Y. Inn, *J. Non.-Cryst. Solids* **2006**, *352*, 4464.
[27] J. Deubener, R. Müller, H. Behrens, G. Heide, *J. Non.-Cryst. Solids* **2003**, *330*, 268.
[28] C. Zhou, M. Stepniewska, L. Longley, C. W. Ashling, P. A. Chater, D. A. Keen, T. D. Bennett, Y. Yue, *Phys. Chem. Chem. Phys.* **2018**, *20*, 18291.
[29] M. M. Smedskjaer, R. E. Youngman, S. Striepe, M. Potuzak, U. Bauer, J. Deubener, H. Behrens, J. C. Mauro, Y. Yue, *Sci. Rep.* **2014**, *4*, 3770.
[30] P. G. Debenedetti, F. H. Stillinger, *Nature* **2001**, *410*, 259.
[31] L. M. Wang, V. Velikov, C. A. Angell, *J. Chem. Phys.* **2002**, *117*, 10184.
[32] D. L. Sidebottom, *Front. Mater.* **2019**, *6*, 144.
[33] I. Gallino, *Entropy* **2017**, *19*, 483.
[34] A. Qiao, T. D. Bennett, H. Tao, A. Krajnc, G. Mali, C. M. Doherty, A. W. Thornton, J. C. Mauro, G. N. Greaves, Y. Yue, *Sci. Adv.* **2018**, *4*, eaao6827.
[35] R. Böhmer, K. L. Ngai, C. A. Angell, D. J. Plazek, *J. Chem. Phys.* **1993**, *99*, 4201.
[36] M. M. Smedskjaer, J. C. Mauro, S. Sen, Y. Yue, *Chem. Mater.* **2010**, *22*, 5358.
[37] W. E. Bull, S. K. Madan, J. E. Willis, *Inorg. Chem.* **1963**, *2*, 303.
[38] P. Richet, B. O. Mysen, D. Andrault, *Phys. Chem. Miner.* **1996**, *23*, 157.
[39] G. Rayner-Canham, T. Overton, *Descriptive Inorganic Chemistry*, W. H. Freeman and Company, New York **2013**.
[40] F. A. Cotton, D. M. L. Goodgame, M. Goodgame, *J. Am. Chem. Soc.* **1961**, *83*, 4690.
[41] Y. Abe, M. Morikawa, M. Kikukawa, *Polyhedron* **1988**, *7*, 2135.
[42] R. Gaillac, P. Pullumbi, K. A. Beyer, K. W. Chapman, D. A. Keen, T. D. Bennett, F. X. Coudert, *Nat. Mater.* **2017**, *16*, 1149.
[43] J. I. Gersten, F. W. Smith, *The Physics and Chemistry of Materials*, Wiley, New York **2001**.
[44] W. Liu, S. J. Borg, D. Testemale, B. Etschmann, J. L. Hazemann, J. Brugger, *Geochim. Cosmochim. Acta* **2011**, *75*, 1227.
[45] T. W. Swaddle, L. Fabes, *Can. J. Chem.* **1980**, *58*, 1418.
[46] H. S. R. Gilson, M. Krauss, *J. Phys. Chem. A* **1998**, *102*, 6525.
[47] S. F. Lincoln, D. T. Richens, A. G. Sykes, in *Comprehensive Coordination Chemistry II* (Eds: J. A. McCleverty, T. J. Meyer), Elsevier, Amsterdam **2003**, pp. 515–555.
[48] A. H. Slavney, H. K. Kim, S. Tao, M. Liu, S. J. L. Billinge, J. A. Mason, *J. Am. Chem. Soc.* **2022**, *144*, 11064.
[49] Z. Yin, Y. Zhao, S. Wan, J. Yang, Z. Shi, S. Peng, M. Chen, T. Xie, T. Zeng, O. Yamamuro, M. Nirei, H. Akiba, Y. Zhang, H. Yu, *J. Am. Chem. Soc.* **2022**, *144*, 13021.
[50] A. M. Bumstead, M. F. Thorne, T. D. Bennett, *Faraday Discuss.* **2021**, *225*, 210.
[51] M. M. Smedskjaer, J. C. Mauro, Y. Yue, *Phys. Rev. Lett.* **2010**, *105*, 115503.
[52] Y. Yang, C. J. Wilkinson, K. H. Lee, K. Doss, T. D. Bennett, Y. K. Shin, A. C. T. Van Duin, J. C. Mauro, *J. Phys. Chem. Lett.* **2018**, *9*, 6985.
[53] K. Yang, B. Yang, X. Xu, C. Hoover, M. M. Smedskjaer, M. Bauchy, *J. Non-Cryst. Solids* **2019**, *514*, 15.
[54] M. Stepniewska, K. Januchta, C. Zhou, A. Qiao, M. M. Smedskjaer, Y. Yue, *Proc. Natl. Acad. Sci. USA* **2020**, *117*, 10149.
[55] R. Conradt, *J. Am. Ceram. Soc.* **2008**, *91*, 728.
[56] S. S. Sørensen, E. J. Pedersen, F. K. Paulsen, I. H. Adamsen, J. L. Laursen, S. Christensen, H. Johra, L. R. Jensen, M. M. Smedskjaer, *Appl. Phys. Lett.* **2020**, *117*, 031901.